Recycling of laser and plasma radiation energy for enhancement of extreme ultraviolet sources for nanolithography

V. Sizyuk,[1] T. Sizyuk,[1] A. Hassanein,[1] and K. Johnson[2]
[1]*Center for Materials under Extreme Environment (CMUXE), School of Nuclear Engineering Purdue University, West Lafayette, Indiana 47907, USA*
[2]*KJ Innovation, 2502 Robertson Rd., Santa Clara, California 95051, USA*

(Received 15 September 2017; accepted 17 December 2017; published online 5 January 2018)

We have developed comprehensive integrated models for detailed simulation of laser-produced plasma (LPP) and laser/target interaction, with potential recycling of the escaping laser and out-of-band plasma radiation. Recycling, i.e., returning the escaping laser and plasma radiation to the extreme ultraviolet (EUV) generation region using retroreflective mirrors, has the potential of increasing the EUV conversion efficiency (CE) by up to 60% according to our simulations. This would result in significantly reduced power consumption and/or increased EUV output. Based on our recently developed models, our High Energy Interaction with General Heterogeneous Target Systems (HEIGHTS) computer simulation package was upgraded for LPP devices to include various radiation recycling regimes and to estimate the potential CE enhancement. The upgraded HEIGHTS was used to study recycling of both laser and plasma-generated radiation and to predict possible gains in conversion efficiency compared to no-recycling LPP devices when using droplets of tin target. We considered three versions of the LPP system including a single CO_2 laser, a single Nd:YAG laser, and a dual-pulse device combining both laser systems. The gains in generating EUV energy were predicted and compared for these systems. Overall, laser and radiation energy recycling showed the potential for significant enhancement in source efficiency of up to 60% for the dual-pulse system. Significantly higher CE gains might be possible with optimization of the pre-pulse and main pulse parameters and source size. *Published by AIP Publishing.*
https://doi.org/10.1063/1.5004980

I. INTRODUCTION

Commercial extreme ultraviolet (EUV) lithography systems use laser-produced plasma (LPP) sources to generate EUV radiation.[1–3] The near-term source power requirement for high-volume manufacturing (HVM) is 250 W at intermediate focus (IF) within a 2% wavelength band centered at 13.5 nm. In the longer term, power levels of 500 W or more will be required to achieve high productivity and also to minimize the impact of shot noise in the lithographic printing process.[4–6]

The primary strategies being pursued to increase LPP power are to increase the drive laser power (e.g., to 40 kW) or to possibly use a free-electron laser (FEL)[7] and various hybrid devices.[8–11] An alternative, simpler, and more practical approach would be to improve EUV conversion efficiency (CE) by recycling unused out-of-band (OoB) radiation back to the plasma via reflective optics. This method was first proposed by Bayraktar *et al.*,[12] and Johnson[13,14] improved the method to greatly increase recycling efficiency and also provide spectral filtering capability.

In this paper, we present the first published plasma-physics analysis of LPP power recycling. Preliminary results, based on the High Energy Interaction with General Heterogeneous Target Systems (HEIGHTS) simulation package, indicate that a 60% or higher CE gain may be achievable with commercial (dual-pulse) systems. Further work will be required to refine the model and to optimize the LPP system for maximum power performance, but the preliminary data are indicative of the potential of power recycling.

Section II describes the power-recycling optical system and outlines some of the assumptions and simplifying approximations underlying the plasma-physics simulation. Section III details the mathematical model of the plasma physics and describes how HEIGHTS was adapted to accommodate power recycling. Section IV discusses the simulation results, and Sec. V summarizes the conclusions of this study.

II. POWER-RECYCLING OPTICS

Plasma-generated and scattered radiation can be directed back to the plasma by retroreflective mirrors to effect power recycling.[13,14] This includes most of the radiation that does not intercept the collection mirror, which can be retroreflected by means of spherical mirrors centered on the plasma. However, this approach could be problematic because the plasma's retroreflected self-image would be inverted. For example, the front (laser-facing) side of the plasma would be imaged to the back side, which faces away from the collector. EUV collection would be more efficient if the recycled radiation were concentrated on the front (collector-facing) plasma surface. Also, any positional displacement of the plasma would cause the reflected image to move in the opposite direction, resulting in EUV power fluctuations from positional instabilities.

These problems can be avoided by designing the recycling optics to form a non-inverted plasma self-image. One

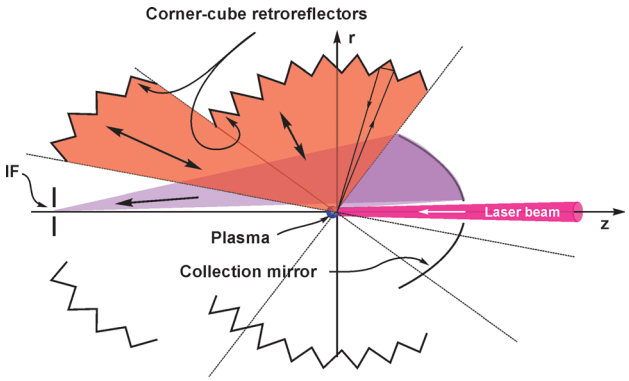

FIG. 1. Power-recycling radiation outside of the collector optical path. The OoB and laser radiation are returned back to emission and reflection points.

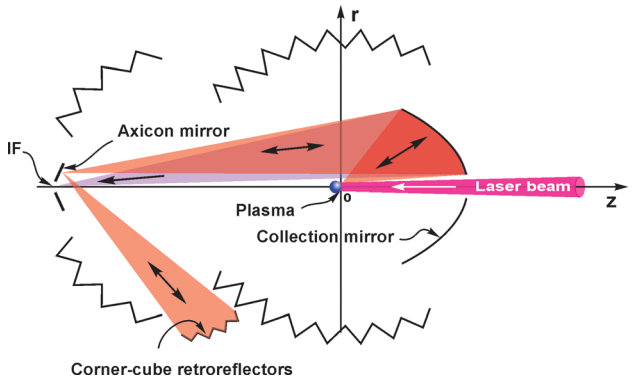

FIG. 3. Power-recycling radiation intercepting the collector. Axicon mirror redirects OoB and laser radiation for retroreflection back to plasma.

approach is to use corner-cube reflectors, as illustrated in Fig. 1. EUV output from the laser-irradiated plasma is focused by the collection mirror into an intermediate-focus (IF) aperture, and OoB radiation outside of the collector optical path is retroreflected by an array of corner-cube elements. The corner cubes are depicted schematically in Fig. 1 as two-surface reflectors, shown in cross section (e.g., see illustrative ray in the figure), but they are actually three-surface reflectors with slightly curved surfaces to accommodate the beam's wavefront curvature.[14]

Much of the OoB radiation intercepting the collector—especially the scattered laser power—can also be recycled. The power-recycling optics are adapted from a collector design that provides broadband spectral purity filtering via grating diffraction. (In effect, the LPP source operates as an EUV grating monochromator.) As illustrated in Fig. 2, the mirror shape is designed to focus plasma radiation onto a ring or halo surrounding the IF aperture—not onto the IF itself as in a conventional design. A blazed diffraction grating on the mirror efficiently diffracts in-band EUV into the aperture, while diffracted OoB radiation is directed out of the aperture via chromatic dispersion. The undiffracted and diffracted OoB radiation are both fully excluded from the IF aperture.

Most of the OoB radiation is concentrated in the undiffracted (zero-order) beam, which can be retroreflected back to the plasma. As illustrated in Fig. 3, a small axicon mirror located at or near the zero-order ring focus expands the OoB beam and separates it from the EUV optical path so that the OoB radiation can be retroreflected by a corner-cube mirror array. (Positioning the corner cubes right at or close to the ring focus, without the axicon expander, could be problematic because the span of ray angles at the reflector would be very large.) The axicon could be an actively cooled molybdenum element, which can withstand the concentrated radiation levels.

For the present study, a recycling mechanism approximating the corner-cube system is assumed. As illustrated in Fig. 4, any plasma-emitted or scattered photons directed along a particular optical ray path are assumed to return to the plasma along the same ray, in the opposite direction, with a defined optical efficiency (probability of return). The ray angle relative to the laser beam axis is denoted as Θ, and the recycling optics are characterized by the retroreflection efficiency as a function of Θ and wavelength.

The optical systems illustrated in Figs. 1 and 3 can be used to recycle either plasma-produced radiation or plasma-scattered laser radiation, or both. Figure 5 illustrates the reflection efficiencies of several reflector types (at near-normal incidence): an enhanced aluminum mirror (100 nm MgF_2 on Al), a bare molybdenum mirror (such as the axicon), and a blazed, conformal-multilayer EUV grating[13] with 50 Mo/Si bilayers (the collector). The efficiencies are all quite high (greater than 97%) at the 10.6-μm laser wavelength but drop off significantly below 2 μm. The efficiency loss would be compounded by the number of reflections [three for a corner cube, plus two axicon reflections and two collector reflections for the collector light path (Fig. 3)]. To simplify preliminary analysis, two recycling conditions were simulated to approximately bracket the possible range of mirror efficiencies: for the first simulation, a compound mirror efficiency of 90% is assumed over the full OoB range, and for the second simulation the efficiency is assumed to be

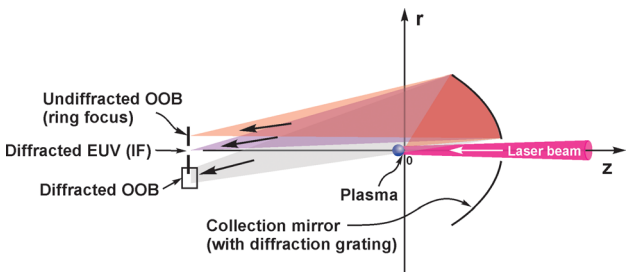

FIG. 2. Spectral-purity filtering via grating diffraction. In-band EUV is directed into IF; all other radiation is excluded.

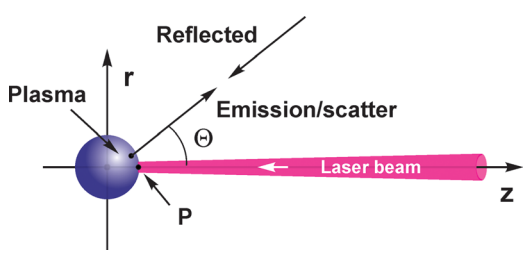

FIG. 4. Ray retroreflection in simulation. Recycled radiation is returned back to the emission point.

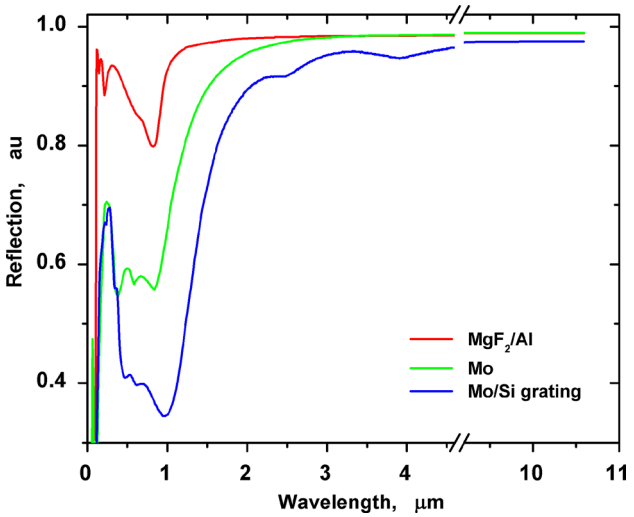

FIG. 5. Reflection efficiencies (single-surface, near-normal incidence) of various reflector types.

90% at the 10.6-μm laser wavelength and zero at all other OoB wavelengths. The recycling calculations were provided and compared for three angular collection ranges of $10^\circ < \Theta < 80^\circ$, $60^\circ < \Theta < 120^\circ$, and $10^\circ < \Theta < 170^\circ$. (The simulation results are discussed in Sec. IV.)

The above assumptions are coarse approximations, which will need to be refined based on detailed specifications of the mirror surface geometry and reflection coatings. Future simulation work will be required to fully characterize the plasma's scattering/emission spectrum, upon which the optical design will be based. But it is clear from Fig. 5 that full-spectrum, vacuum ultraviolet (VUV)-to-IR reflectance can be achieved with a simple MgF_2/Al mirror outside of the collector light path. For the collector light path, significant reflectance below 200 nm might not be possible without major efforts in optical coating and material optimization.

One issue of concern is the effect of condensing plasma debris on the power-recycling mirrors. The sensitivity of OoB reflection to tin deposition has not yet been studied, but if it is no more sensitive than EUV reflection, then this would probably not be a major problem because the power-recycling mirrors would be relatively simple and inexpensive compared to the EUV collector. (For example, the corner-cube mirrors could be electroplated replica optics.)

III. MATHEMATICAL AND PHYSICAL MODELS

A combination of both laboratory experiments and computer simulation modeling can provide a complete picture of plasma evolution and determine the full impact of various physical processes involved. Preliminary computer simulations greatly reduce the time and cost of development and, in many cases, clarify the theoretical limits of potential new device ideas and parameters. The comprehensive computer code HEIGHTS (High Energy Interaction with General Heterogeneous Target Systems) has been successfully developed and benchmarked at Purdue CMUXE (Center for Materials Under eXtreme Environments) over the years to analyze various aspects of plasma physics phenomena.[15–18]

The HEIGHTS integrated package combines state-of-the art full 3D models of energy deposition, vapor/plasma formation/evolution and magnetohydrodynamic (MHD) processes, thermal conduction in materials and in plasma, atomic physics and resulting opacities, detailed photon radiation transport, and interaction between plasma/radiation and target materials.

To develop integrated physical models of plasma development and evolution, the hierarchy of all involved physical processes and detail mechanisms for the incorporation of these processes should be analyzed, tested, and benchmarked. For this reason, HEIGHTS models were created from the basic principles of plasma/particle/radiation interaction with target materials and do not include any fitting parameters or extrapolating physics from other sources. The package consists of set of independent modules that describe the main processes taking place in laboratory plasma devices. Some processes, such as laser photons deposition, photon radiation transport, and thermal conduction in plasma, have several implementations that allow comparison of various methods on modeling results and enable high efficiency with optimization of computer time. The major physics blocks of the package are shown in Fig. 6.

As shown in Fig. 6, the main component of the HEIGHTS package is the MHD block, which has been updated for simulating LPP devices with power-recycling mirrors. Since we consider LPP systems at millimeter-size range and the cumulative vaporized particle density is estimated to be higher than $10^{17}\,\mathrm{cm}^{-3}$, the hydrodynamic approach implemented in HEIGHTS package is valid for this study.[19] The general form of the hydrodynamic equation set in two-temperature approximation consists of the following components:

$$\begin{aligned}
&\frac{\partial \rho}{\partial t} + \nabla \cdot (\rho \mathbf{v}) = Q_{mvap},\\
&\frac{\partial \rho \mathbf{v}}{\partial t} + \nabla \cdot (\rho \mathbf{v}\mathbf{v} + p_t) = 0,\\
&\frac{\partial e_t}{\partial t} + \nabla \cdot [\mathbf{v}(e_t + p_t)] = Q_{evap} + Q_{RT} + Q_{HC} + Q_{Las} + Q_{Mir},\\
&\frac{\partial e_e}{\partial t} + \nabla \cdot [\mathbf{v}(e_e + p_e)] = Q_{ei} + Q_{RT} + Q_{HC} + Q_{Las} + Q_{Mir},
\end{aligned} \tag{1}$$

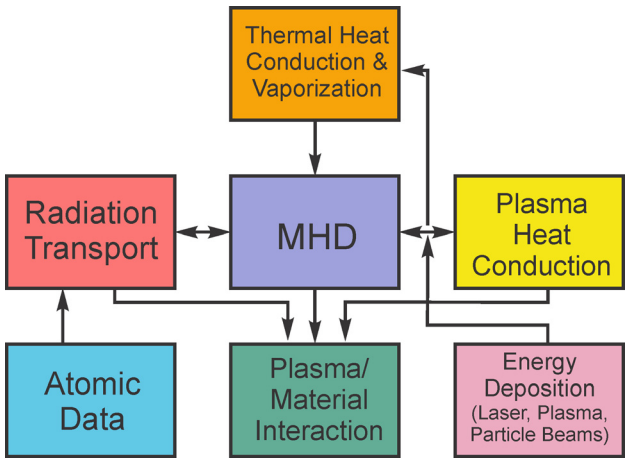

FIG. 6. Block diagram of the HEIGHTS models and computer package.

where we separated the electronic part of total energy into the individual equation. Here, $e_t = e_i + e_e + e_k$ is the total energy, e_e is the electronic component of the plasma energy, which includes the thermal energy of electrons and ionization energy, e_i is the ion component of the plasma energy, and $e_k = \rho v^2/2$ is the kinetic energy of the plasma. Similar to the energy, pressure also has electron and ion parts: $p_t = p_e + p_i$. We use here the subscript e for electrons and i for ions. Since Eq. (1) has convective terms such as hydrodynamic fluxes and dissipative terms such as heat conduction, laser heating, radiation transport, and electron-ion interaction, we used splitting methods in our numerical algorithm to separate the hyperbolic and parabolic parts.[20] According to this method, the main dissipation processes (see Fig. 1) are presented in Eq. (1) as right hand terms, i.e., sources: Q_{mvap} and Q_{evap} are the density and the energy sources from the target vaporization; Q_{Las} is the energy input from laser absorption; Q_{Mir} is the radiation energy reflected back onto the plasma by the mirrors; Q_{RT} and Q_{HC} are the energy redistributions due to radiation transport and heat conduction, respectively. The electron-ion interaction term Q_{ei} is described in detail in Ref. 19.

The computation model currently does not include any time delay between scatter/emission and reabsorption of the recycled energy (Q_{Mir}). Future work will take into account the time delay along the recycling optical paths due to the finite light speed (300 mm/ns).

The LPP modeling was performed using a cylindrical geometry where the azimuthal components of all parameters are integrated due to the invariability of the laser beam in this direction. The axial and radial cylindrical coordinates are indicated as z and r in Fig. 4. Since plasma parameters are assumed invariable along the azimuthal (φ) direction, all function derivatives with respect to φ are zero.

The recycling optics are assumed to be symmetric and have a collecting angle defined by Θ limits (Fig. 4). The target is chosen to be a spherical droplet. Equation (1) can be expressed in a matrix form for the chosen coordinate system with the implementation of the total variation diminishing scheme in Lax-Friedrich formulation (TVD-LF)[18,21]

$$\frac{\partial \mathbf{U}}{\partial t} + \frac{1}{r}\frac{\partial}{\partial r}[r\mathbf{F}(\mathbf{U})] + \frac{\partial \mathbf{P}(\mathbf{U})}{\partial r} + \frac{\partial \mathbf{G}(\mathbf{U})}{\partial z} = \mathbf{\Omega}, \tag{2}$$

where the hydrodynamic fluxes are

$$\mathbf{U} = \begin{bmatrix} \rho \\ \rho v^r \\ \rho v^z \\ e_t \\ e_e \end{bmatrix} \quad \mathbf{F}(\mathbf{U}) = \begin{bmatrix} \rho v^r \\ \rho v^r v^r \\ \rho v^z v^r \\ v^r(e_t + p_t) \\ v^r(e_e + p_e) \end{bmatrix}$$

$$\mathbf{P}(\mathbf{U}) = \begin{bmatrix} 0 \\ p_t \\ 0 \\ 0 \\ 0 \end{bmatrix} \quad \mathbf{G}(\mathbf{U}) = \begin{bmatrix} \rho v^z \\ \rho v^r v^z \\ \rho v^z v^z + p_t \\ v^z(e_t + p_t) \\ v^z(e_e + p_e) \end{bmatrix}, \tag{3}$$

and the dissipative terms are accumulated in the source-matrix

$$\mathbf{\Omega} = \begin{bmatrix} Q_{mvap} \\ 0 \\ 0 \\ Q_{evap} + Q_{RT} + Q_{HC} + Q_{Las} + Q_{Mir} \\ Q_{ei} + Q_{RT} + Q_{HC} + Q_{Las} + Q_{Mir} \end{bmatrix}. \tag{4}$$

In the HEIGHTS simulation of LPP devices, the numerical modeling was focused on the integration of main physical processes responsible for the generation of the plasma and plasma radiation. The main source component of this modeling uses Monte Carlo methods for the simulation of laser photon absorption, reflection, and reabsorption. The laser beam is considered as a directional flux of "macro" photons. The individual macro-photon has the same properties (absorption, reflection probability, etc.) of the real "one" laser radiation photon. However, the action of each real photon cannot be individually simulated because of the large number of real/actual photons in the beam. The action (energy transport, etc.) of each group photon is combined into the macro-photon action. The weight of one macro-photon, W_{macro}, is estimated from the actual number of photons in the laser pulse and the number of macro-photons that are needed for reasonable calculation time and accuracy[15]

$$W_{macro} = \frac{N_{real}}{N_{macro}}, \quad N_{real} = \frac{P_{las}}{E_{ph}}, \tag{5}$$

where P_{las} is the incident laser power and E_{ph} is the energy of one real laser radiation photon.

After vapor heating and plasma cloud formation, a three-medium, self-consistent system evolves under the laser beam exposure. For the first medium, liquid tin, the target surface's reflection coefficient k_{target} can be derived from the optical surface properties based on the Drude theory[22]

$$k_{target} = \frac{(n-1)^2 + k^2}{(n+1)^2 + k^2}. \tag{6}$$

Calculations of the tin target reflectivity give $k_{target} = 0.84$ for the Nd:YAG laser with $\lambda = 1.064$-μm, and $k_{target} = 0.92$ for the CO_2 laser with $\lambda = 10.64$-μm wavelength, based on the Sn optical data taken from the Ref. 23. The second and third media are a vapor/plasma mixture and a surrounding, well-developed plasma, which require special modeling of laser photon propagation. The detailed description of laser absorption in vapor and plasma can be found in Ref. 24, where the vaporization model is also discussed.

The Monte Carlo approach provides broad capabilities for modeling the recycling mirror operation. Inherently, the mirror action is an additional boundary condition applied to the computational domain for escaping photons, including reflected/scattered laser photons and plasma-generated photons. The mirrors reflect escaping photons back to the plasma with an efficiency k_{mirror}, which is a function of wavelength and emission angle Θ (Fig. 4). We compared two recycling

modes: "R-Recycling," in which the photons are retroreflected as illustrated in Fig. 4, and "P-Recycling," in which the photons are reflected to a single axial point ***P*** on the plasma's laser-facing surface. P-Recycling is not physically realistic (it is not possible to concentrate all the light from an extended source onto a single point) but is intended to explore the hydrodynamic and CE sensitivity to a narrow, focused location of the recycled energy.

The HEIGHTS models for radiation transport used numerical algorithms with weight hierarchy factors of statistically accumulated events. Two main weight factor categories were implemented, i.e., normalization of emitted photon "bundles" relative to the most radiating cell of computational domain and normalization of the photon bundle magnitudes relative to the optical thickness of the cell. The first weight coefficient enables efficient description of the emission process by neglecting emission from cold cells. With the second coefficient, "idle" processes are ignored for the situation when an emitted photon is absorbed within the same cell (absorbed lines). These coefficients allowed significantly reduced computation time for extensive simulation of radiation transport. Additionally, a third weight coefficient was implemented to describe the effect of small cell sizes. The volume of the emitting cell can be so small that the number of calculated photon bundles will be less than one. In this case, the photon bundles are adjusted using the third weight coefficient. More detailed description of plasma radiation transport can be found in our previous publication.[25]

Following the splitting methods used in the HEIGHTS package,[20] the additional dissipative source-terms are calculated separately with the second (dissipative) stage of the solver used then as correctors of the main hydrodynamic module solution (Fig. 6). The size of the time step for the entire integrated LPP simulation is usually limited by one of the various plasma processes involved. One of the most expensive computational parts of the full hydrodynamics problem is modeling heat conduction in plasma where an implicit algorithm is more efficient due to time step requirement. However, heat conduction in solid or liquid matter is much slower in comparison to a similar process in plasma. Overall, the smaller time step required by plasma processes allows implementing explicit methods for modeling heat conduction in solid or liquid targets without any numerical instabilities or noticeable errors. This avoids complex implicit schemes for the simulation of target thermal response to laser beam spatial and temporal profile inputs. Therefore, an explicit method was implemented for the solution of the heat conduction equation in the target, and an implicit scheme, employing the standard linear solver for the sparse matrixes, was used for the plasma heat conduction.[26]

The benchmarking of the above-described models and methods were published in several articles, e.g., results for hydrodynamics scheme,[21,27] for plasma heat conduction block,[20,26] for the plasma-material interaction problem,[28,29] and for Monte Carlo radiation transport algorithm[30,31] showed good agreement with experiments and other theoretical studies. To validate the upgraded HEIGHTS package with new implemented modeling of radiation recycling, we simulated a classical EUV test case with planar tin target[32] with $k_{mirror} = 0$ (i.e., no mirror reflection and recycling) and obtained CE results identical to our previous modeling.[33]

IV. SIMULATION RESULTS

We considered in this study three different cases of laser-target interaction with a tin droplet using optimum laser parameters for efficient EUV generation: (1) a single CO_2 laser, (2) a single Nd:YAG laser, and (3) a double-pulse combination, i.e., Nd:YAG pre-pulse followed by CO_2 as the main driving laser. In all cases, a tin droplet with 50 μm diameter was used as the initial target. The target was located along the z-axis in such a way that the droplet's laser-facing axial surface point ***P*** (Fig. 4) corresponded to the axis origin $z = 0$. Temporal and spatial intensity distributions of laser pulse had a Gaussian profile.[18] The laser intensity, spot size, and pulse duration varied for different laser wavelengths. The CO_2 laser had spot diameter of 100 μm and pulse duration of 30 ns, whereas Nd:YAG laser had a smaller diameter of 50 μm and a pulse duration of 20 ns.

Preliminary simulations were conducted to determine where mirrors should be located to maximize the return of photons escaping the target/plasma domain. Calculation of the angular distribution of the escaping radiation at domain borders showed the potential for future optimization of the recycling mirrors.

Figure 7 illustrates the total escaped angular spectrum of the radiation intensity as a function of emission angle Θ (Fig. 4). We show separate angular spectra for (a) laser radiation and (b) plasma-generated radiation. Figure 7 also illustrates the recycling band for mirrors covering an angular range $60^\circ < \Theta < 120^\circ$, denoted as the "60°/120°" configuration later in this paper. We also considered, for comparison, another mirror configuration, 10°/80°, which is more effective based on the angular distribution shown in Fig. 7. For the dual-pulse system, a third configuration, 10°/170°, was simulated to test performance at the upper limits of the collection range.

The first preliminary simulations, for the CO_2 laser and the 60°/120° mirror configuration, with $k_{mirror} = 1$ at all OoB wavelengths, showed that the return of the escaped radiation back into the laser-target interaction area can have a significant impact on the plasma hydrodynamics evolution and plasma characteristics. Figure 8 shows calculated plasma temperature (color palette) and density (white contours) fields with and without radiation recycling. This will have pronounced effect of EUV production and source size as explained below.

Plasmas produced from CO_2 laser interaction with small droplets have higher recycling potential, in comparison to Nd:YAG, due to the higher reflection from solid/liquid tin and less absorption at the CO_2 wavelength in the developed plasma. Thus, a larger portion of the radiation energy can be returned back. Figure 8 shows results of CO_2 laser interaction with a tin droplet using laser intensity of $I = 2 \times 10^{10}$ W/cm^2 and pulse duration of $\tau = 30$ ns. Figure 8(b) was calculated assuming P-Recycling, i.e., all escaped laser and plasma-generated radiation within the emission range $60^o < \Theta < 120^o$ is directed back toward the axial focus point ***P*** at the zero point, $z = 0$. The figure illustrates a

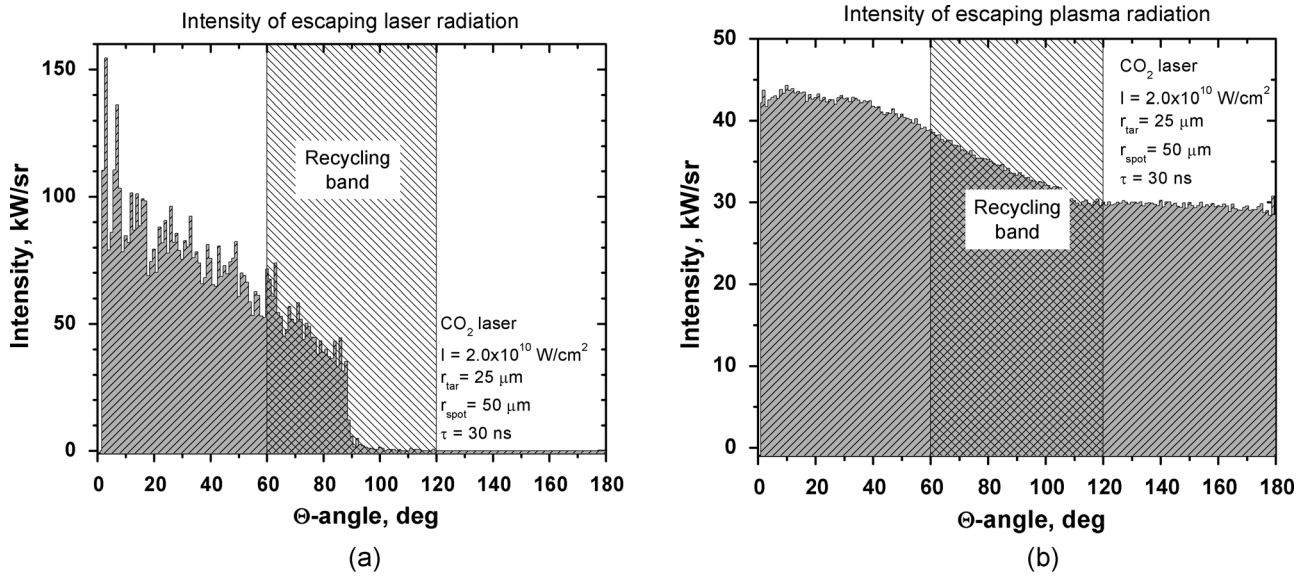

FIG. 7. Angular distribution of escaping radiation intensity scaled per solid angle unit: (a) laser photons and (b) plasma-generated radiation.

drastic acceleration of the target surface vaporization processes and increasing of the vapor/plasma plume above the target with relatively low temperatures. The area with maximum temperature as well as the area with optimum temperatures for EUV emission is located ∼50 μm further from the target surface in comparison with non-recycling LPP. Figure 8(b) also shows that the recycled radiation can cause major changes in the established hydrodynamic area [Fig. 8(a)] where the laser light—EUV conversion is initially optimized. We conclude here that the recycled radiation parameters such as the amount of recycled energy and focusing point/area can have significant effect on the re-radiation processes, which can either greatly enhance the CE or in some cases even negatively influence the final efficiency.

The influence of the recycling point on the EUV generation process can be determined from the CE plots as a function of the focusing point/area on z-axis location as shown in Fig. 9. The plot illustrates the CE for P-Recycling, but with the location of the focus point (***P*** in Fig. 4) varied along the z axis.

Results in Fig. 9 illustrate the nonlinear character of the recycling processes. The red line shows the CE for the case of non-laser out-of-band radiation recycling only, and the blue line demonstrates the CE for laser radiation recycling only. The pink straight line shows the simulated CE without any recycling. The black line, i.e., the CE for all out-of-band recycling (laser and plasma radiation) is not just the sum of the red and blue curves. Moreover, the shape of the blue curve indicates that focusing the radiation on the opposite side of target (facing away from the laser) is more effective in increasing the CE in the case of laser-only radiation recycling. Overall, the maximum in the CE increase achieved in these simulations was from ∼1.0% (no recycling basic case) up to ∼1.56% using total recycling focused at the zero point (front of the initial droplet location). The final CE was increased ∼55% (but with the caveat, as noted in Sec. III,

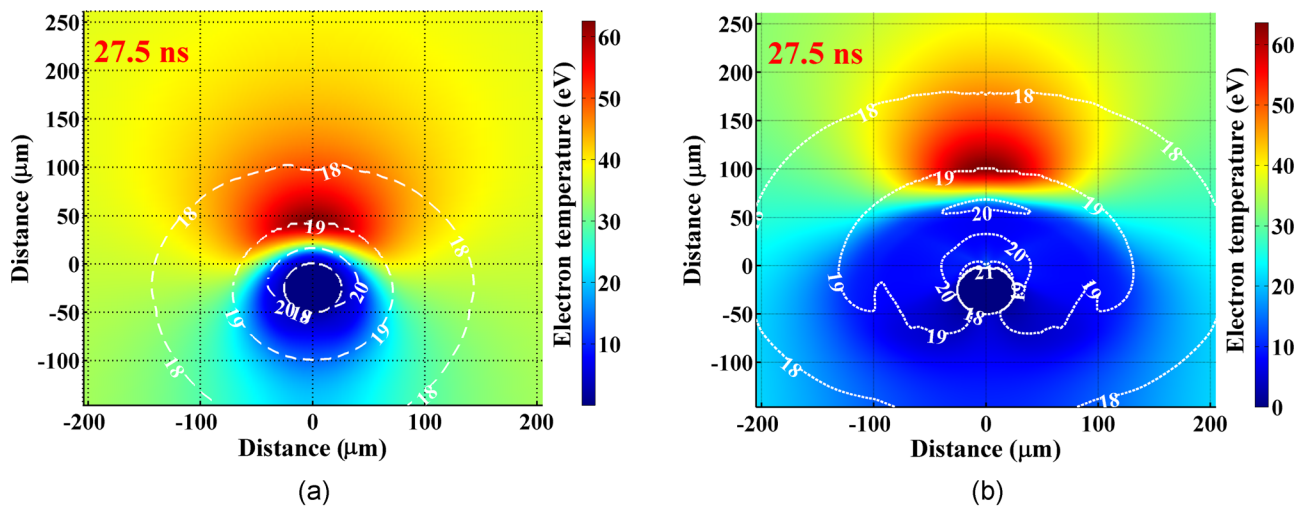

FIG. 8. Effect of recycling all out-of-band radiation (laser and plasma-generated): (a) no recycling and (b) with recycling (z is vertical; r is horizontal).

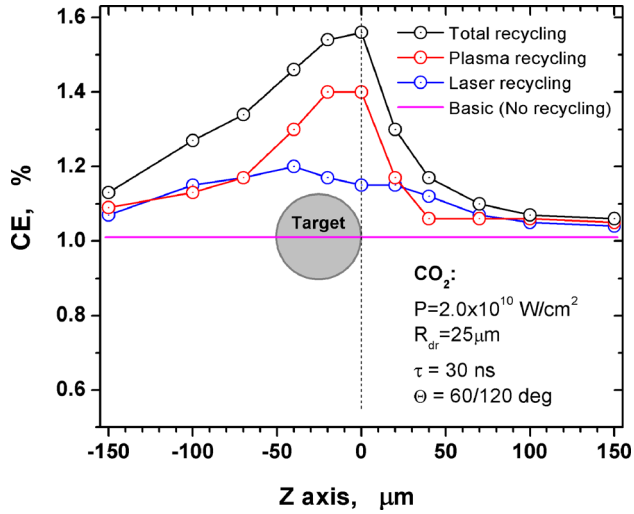

FIG. 9. Dependence of CE on CO_2 laser radiation recycling as function of mirror focus location along Z-direction.

that P-Recycling is an idealization that is not physically realizable).

In the process of HEIGHTS full simulations, the energy balance and energy distribution during the pulse were recorded. Figure 10 shows the energy balance for basic, non-recycling option (left) and for the P-Recycling with the focus point $\boldsymbol{P}$ at $z = 0$ (right). The energy generated by laser pulse is shown by the black curve.

The upper purple band shows the escaped laser energy, i.e., laser photons that were registered outside the computational domain without any interactions and reflections. These are photons which missed the target due to the two times larger laser spot size ($r_{spot} = 50\,\mu$m) than the initial Sn target diameter ($r_{tar} = 25\,\mu$m). In the non-recycling case, the escaped energy reached ∼11.5% of the total laser energy, whereas in the case of recycling mirror case only ∼5.2% of energy escaped due to the larger plasma plume developed by recycled radiation. Figure 10(b) also shows the net amount of laser energy returned to the domain, indicated by the "Back Las. ∼6.4%." The red band shows the final lost laser photons, which were reflected from the target and plasma and were not recycled. Using of the 60°/120° mirror decreased this loss from ∼24% to ∼16%, redirecting a significant part of laser energy to the reabsorption area. The blue bands indicate that the direct absorption of laser photons remains the same for both cases: ∼40% for basic, and ∼41% for recycling. For the reference and comparison, the hatch-shaded band in Fig. 10(a) ("Radiated: 23.3%") shows the total plasma radiation energy, escaped from the domain, that can potentially be returned. The hatch-shaded band in Fig. 10(b) ("Back RT: 20.3%") illustrates out-of-band plasma radiation that was reflected by the mirror.

In contrast to the CO_2 laser case, the Nd:YAG laser radiation has much smaller reflection coefficient at the target surface and higher absorption in the developed laser plasma. The reflection and reabsorption bands for laser radiation are smaller than ∼1.0% for the Nd:YAG laser, and the recycling of out-of-band plasma radiation mainly determines the effect of the recycled energy on the EUV efficiency.

The mirror design will play the most important role in recycling processes. Figure 11 for the Nd:YAG laser is similar to Fig. 9 for the CO_2 laser and shows the CE dependences on the focusing point for two types of the mirror collection angles, i.e., 60°/120° and 10°/80° angle span. The 10°/80° mirror returns more plasma radiation to the focusing point $z = 0$ and increases the final CE from the basic level (without any recycling) of ∼1.5% to ∼1.95%, i.e., the final CE gain was ∼28%.

From the above, we can conclude that in both CO_2 and Nd:YAG cases, the conversion efficiency can be increased greatly by the recycling of the escaping laser and plasma radiation. It is obvious also that the CE increase is higher in the case of ideal conditions of radiation focusing on the target surface, facing laser beam. The 10°/80° mirror is more efficient in comparison with the 60°/120° mirror.

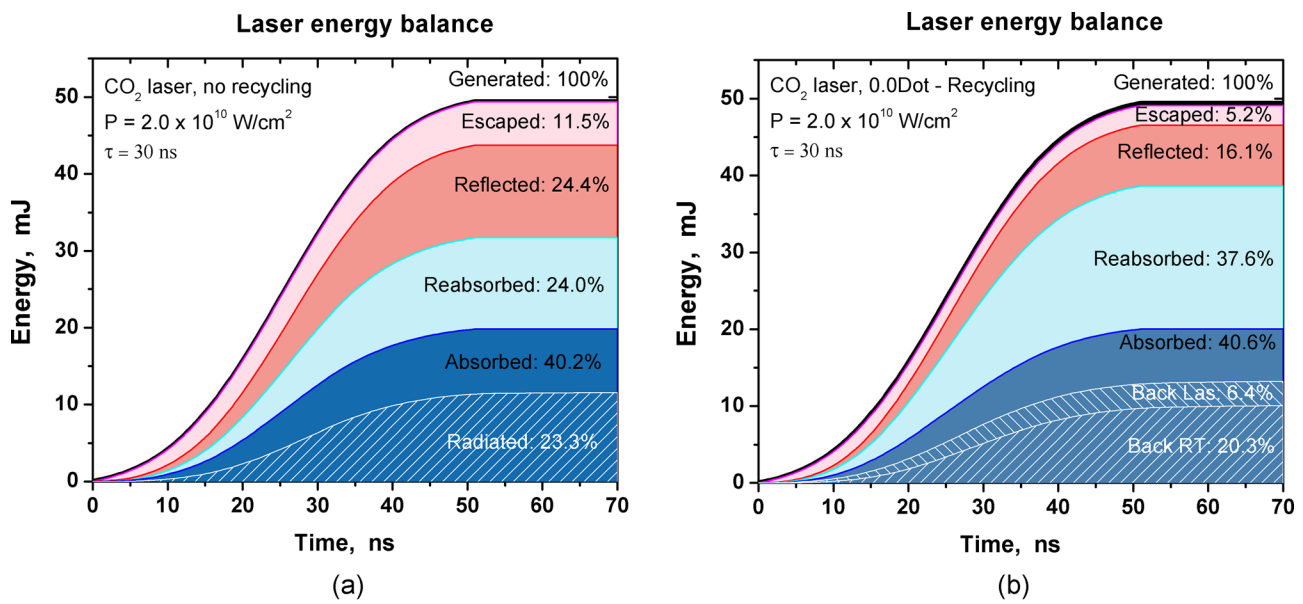

FIG. 10. Energy balance in domain: (a) no recycling and (b) recycling focused at zero point.

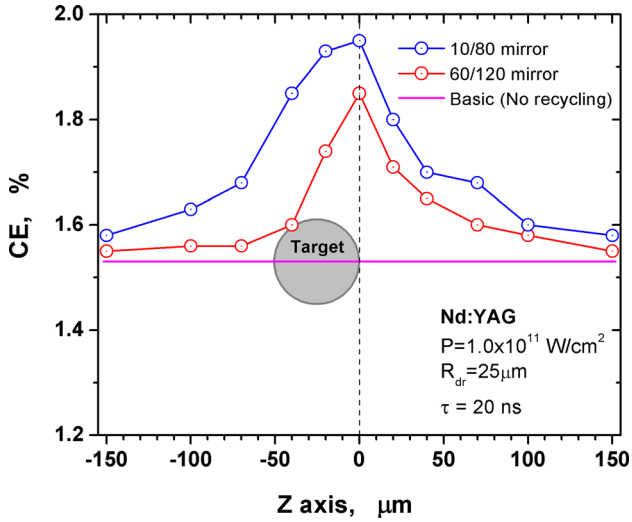

FIG. 11. CE dependence of Nd:YAG laser radiation recycling on mirror parameters.

Figure 12 shows summary of HEIGHTS simulations for the recycling analysis in the range of laser intensities commonly used for the EUV sources. The results are shown for the more efficient 10°/80° mirror design and for both CO_2 and Nd:YAG lasers. The red plot corresponds to the ideal P-Recycling case (focusing of the laser and plasma out-of-band radiation toward point ***P*** in Fig. 4). The green plot presents results for the more realistic R-Recycling case (retroreflecting the recycled radiation, as illustrated in Fig. 4). The blue plot is the baseline no-recycling case.

The red plot in Fig. 12(a) shows some deviation from the usual behavior of the CE as a function of laser intensities. In our opinion, the local overheating by P-Recycling at very high CO_2 laser intensities causes enhanced local evaporation, leading to increased EUV radiation area. However, focusing of all recycled radiation into one point on the target surface would not be practically achievable. Currently, we implemented the R-Recycling option to produce more realistic picture of recycling performance. Figure 12 provides a preliminary indication of the potential benefit of recycling. For future investigations, we plan to develop modeling of the mirrors where photons will be reflected from the mirror surfaces with variable reflection coefficients depending on the specific photons wavelength.

Two goals can be achieved with recycling mirrors: (1) Much more EUV energy can be produced, especially in the case of CO_2 laser, or (2) the laser energy can be reduced to produce the same EUV output relative to no-recycling. Figure 13 illustrates the EUV/laser-energy relationship for laser energies in the range of current LPP systems, for the indicated tin droplet sizes.

We also analyzed the effect of radiation recycling in the case of double-pulse lasers, which are currently adopted as the optimum system for higher overall CE. The main purpose of the double-pulse scheme is in the preconditioning of the target material by the first (pre-pulse) laser to create an expanded target for more efficient EUV generation by the following main (CO_2) pulse, as schematically shown in Fig. 14.

Usually, the pre-pulse laser should have a smaller wavelength for deeper penetration into the target for more effective preheating and ablation of the target material. Ideally, a relatively dense spherical vapor/plasma cloud should be prepared in duration 1 and the delay time (see Fig. 14). For this purpose, we used in our simulations a pre-pulse laser with wavelength $\lambda = 0.266\,\mu$m. The laser energy was $Q_{las} = 10$ mJ, which provided laser intensity of $I_{las} = 2.5 \times 10^{10}$W/cm^2 on a tin droplet with radius of $r_{spot} = 25\,\mu$m. The pre-pulse laser duration was $\tau_1 = 20$ ns and the delay between pulses was 500 ns. Since the tin target was preheated during the pre-pulse stage, the intensity of the main pulse should be less than in the case of single-pulse interaction with small droplet. We used for the main pulse a CO_2 laser intensity of $I_{las} = 5.9 \times 10^9$W/cm^2 and a pulse duration of $\tau_2 = 30$ ns. The large spot size with radius $r_{spot} = 250\,\mu$m allowed complete coupling of the expanded plasma cloud following the delay time.

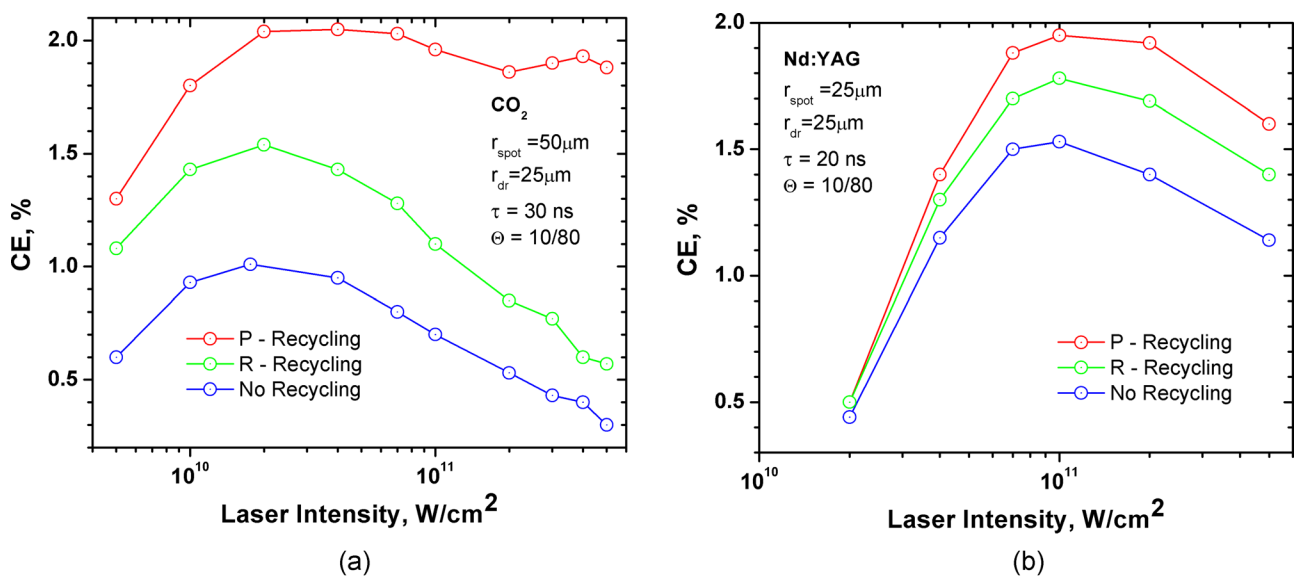

FIG. 12. Dependence of final CE increase on the intensity of: (a) CO_2 laser, (b) Nd:YAG laser.

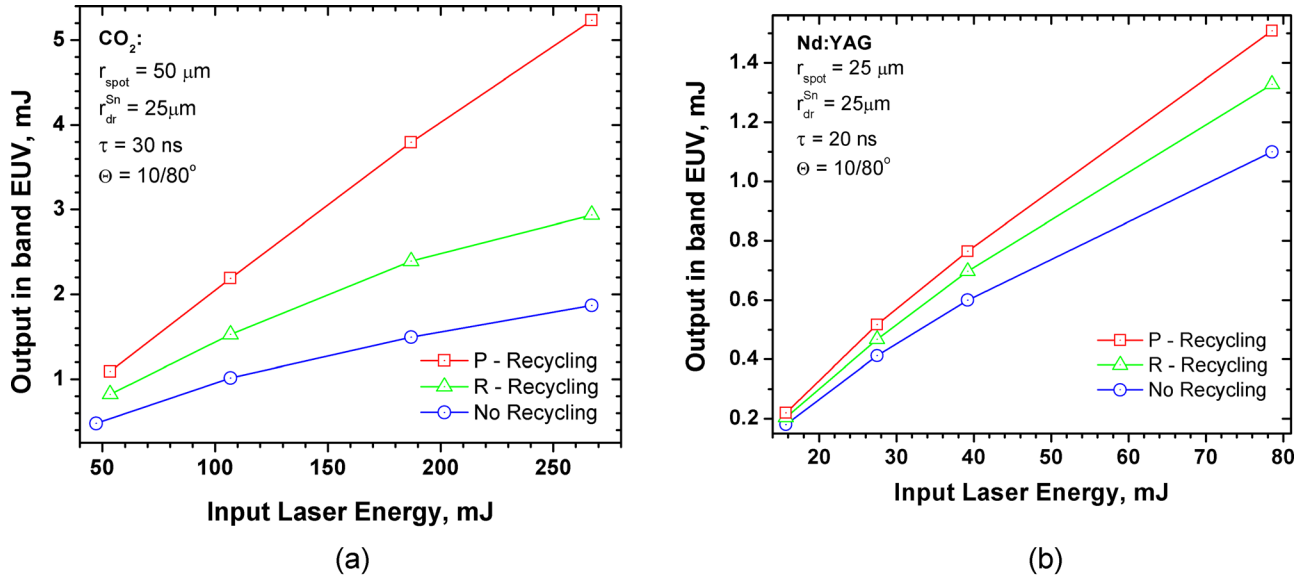

FIG. 13. Recycling benefits for relevant for EUV laser intensities: (a) CO_2 laser; (b) Nd:YAG laser.

Our calculations with these initial parameters showed an increase in CE from the basic single-pulse CO_2 laser CE value of ~1.0% maximum [see Fig. 12(a)] to ~3.0% without any mirror recycling.

Implementing the recycling technique for a double-pulse system requires more accurate adjustment of both lasers, delay time, and the recycling mirrors parameters. HEIGHTS preliminary simulations of this system using R-Recycling, with $k_{mirror} = 1.0$ reflectivity, showed a CE increase up to ~3.8% for the 60°/120° mirror and up to ~3.7% for the 10°/80° mirror. However, when P-Recycling was simulated (again, not a realistic option) under the same conditions, the final CE decreased below ~3.0%. In our opinion, in this case the recycled radiation interfered in preparing of vapor/plasma cloud in the pre-pulse phase, causing the vapor/plasma cloud to become overheated and over-expanded relative to the optimal target size for the CO_2 laser.

This problem could be avoided by reducing the pre-pulse energy and/or reducing the delay time. But to evaluate the effect of recycling on the plasma evolution during the main CO_2 laser pulse, we ran additional simulations with recycling activated only after the pre-pulse delay time (under the premise that the pre-pulse conditions could be re-optimized, with recycling, to produce an expanded target in substantially the same initial condition for the main pulse).

We simulated an extended mirror design with collection angle limits 10°/170° (i.e., $10^o < \Theta < 170^o$) and with R-Recycling (Fig. 4). Two cases were modeled to approximately bracket the range of mirror reflectivities illustrated in Fig. 5. For the first case, the compound mirror reflectivity k_{mirror} is assumed to be 90% over the full OoB spectral range. For the second case, the reflectivity is 90% at the CO_2 laser wavelength (10.6 μm) and zero at all other wavelengths.

Figure 15 shows the EUV source formation in the double-pulse configuration with laser recycling only [Fig. 15(a)] and with the recycling of all OoB radiation [Fig. 15(b)]. The recycling was only applied during the second main pulse, after 520 ns delay, to maintain the same initial state of the vapor/plasma cloud relative to the no-recycling case. This led to an increase in CE of up to 3.1% with laser recycling only (which is similar to the no-recycling case, i.e., 3.0% CE) and 4.8% with recycling of all OoB (about 60% increase from no-recycling). A similar CE enhancement was obtained when the delay time was reduced to create a denser and less expanded plasma plume. The CE increased from 2.7% to 3.9% (with all-OoB recycling) for a 320 ns delay time. While the CE in the case of a shorter delay is smaller, the developed source has a possible advantage in collection efficiency due to the smaller size (Fig. 16) that allows more EUV collection within the given etendue.

Overall, these results showed the potential for significant enhancement in source efficiency, provided that high recycling efficiency can be achieved over the full OoB spectrum, not just at the laser wavelength. Recycling of only laser radiation is not very effective because the expanded target absorbs almost all the CO_2 laser radiation. Recycling of OoB radiation allows a large increase in the plasma volume.

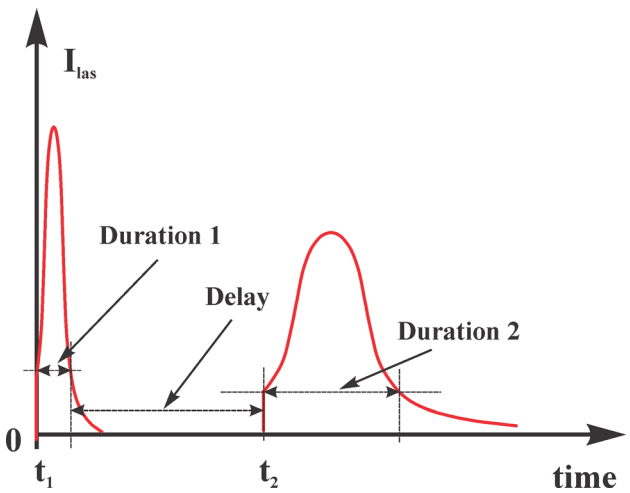

FIG. 14. The double-pulse EUV generation system.

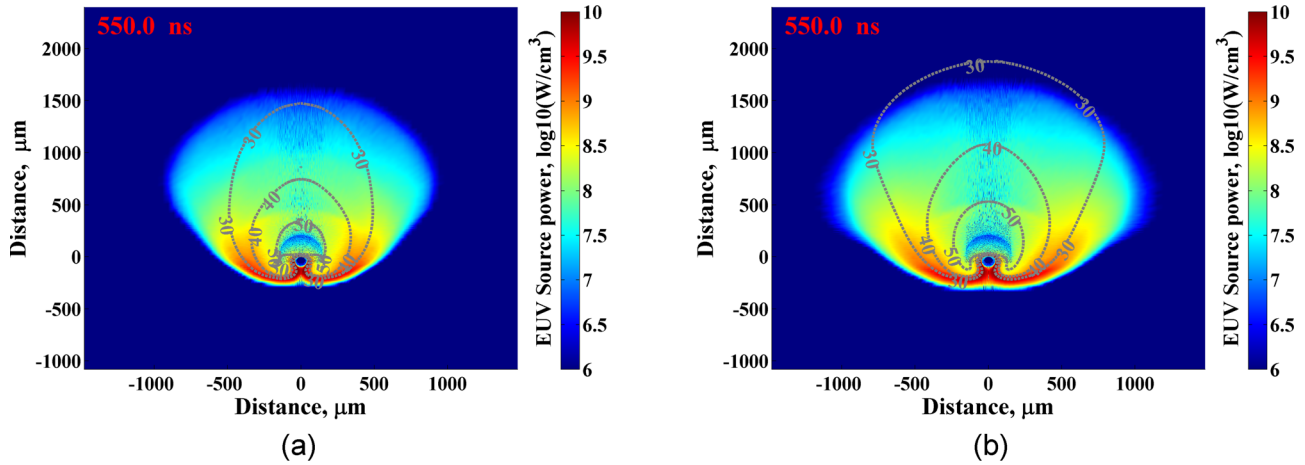

FIG. 15. Snapshot of EUV source produced by the main, CO_2 laser after 520 ns delay with (a) laser radiation recycling only; (b) recycling of all OoB radiation. (Gray contours show electron temperature.)

Further gains in CE might be possible with optimization of the pre-pulse and main pulse parameters, the source size, and the collection and recycling optics.

In general, LPP power recycling could be optimized to significantly enhance EUV generation and/or reduce the required laser power. This becomes even more important as the demand for higher EUV power increases with advances in HVM lithography.

V. CONCLUSIONS

We have developed integrated comprehensive models for accurate simulation of a laser-produced plasma and laser/target interaction including recycling of out-of-band laser and plasma-generated radiation. The power-recycling optics[13,14] include an EUV-diffracting collection mirror, which channels spectrally pure in-band radiation through an intermediate-focus (IF) aperture and through EUV illumination optics. Much of the undiffracted (zero-order) radiation can be reflected back to the collection mirror and onto the plasma, and radiation that does not intercept the collector can also be retroreflected to enhance plasma heating and EUV generation.

The upgraded HEIGHTS package with new enhanced models was used for the first time to study the effect of radiation recycling and potential gain in EUV conversion efficiency (CE) in standard LPP devices. We found that the returning of the escaped radiation back into the laser-target interaction area can have significant impact on plasma hydrodynamics evolution and general plasma characteristics. We simulated three cases of the LPP devices: (1) single CO_2 laser, (2) single Nd:YAG laser, and (3) dual-pulse Nd:YAG + CO_2 laser system. The CO_2 laser device showed a larger potential to increase the CE in comparison to the Nd:YAG laser due to the larger initial reflectivity of the CO_2 radiation from the liquid tin surface and less absorption in the laser plasma. We analyzed laser energy redistribution during the recycling simulation and predicted the CE gain over a broad range single-pulse laser power levels.

Preliminary simulations of dual-pulse LPP device with the recycling option showed an increase in the CE from ~3.0% up to ~4.8% (a 60% gain) without significant optimization, assuming 90%-efficient recycling of all OoB radiation over a 10°–170° angular collection range. In this simulation, recycling was applied only in the main CO_2

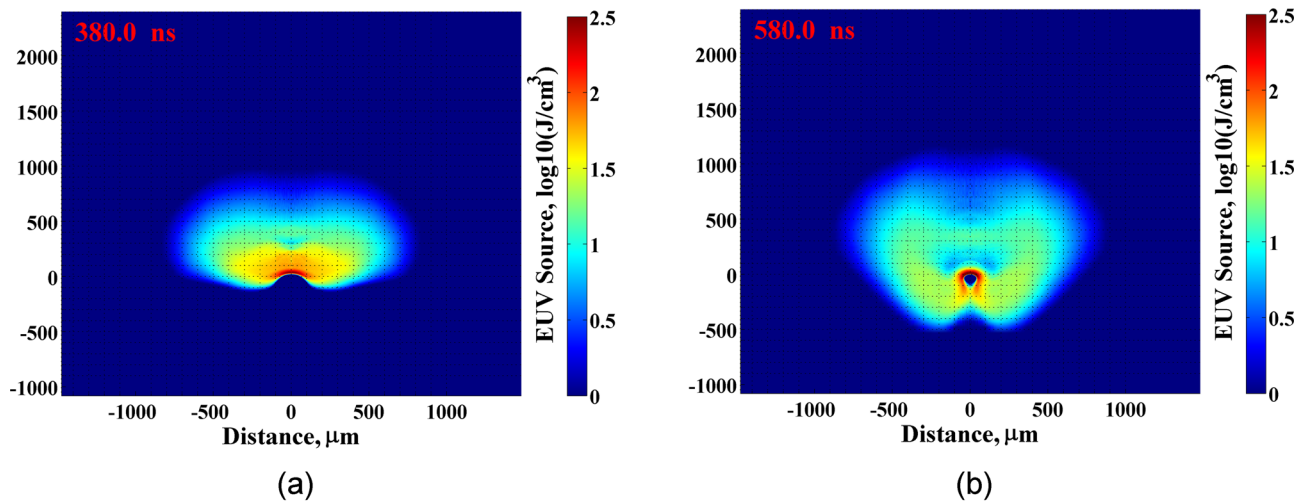

FIG. 16. Time-integrated EUV source produced after (a) 320 ns delay and (b) 520 ns delay.

pulse, not in the pre-pule phase. In practice, the pre-pulse conditions (laser power, delay time) would need to be optimized, with recycling, to avoid overheating and over-expanding the vapor/plasma cloud.

These preliminary results will need to be subsequently refined to improve the accuracy and realism of the simulation (e.g., taking into account the light-speed time delay along the recycling optical paths, variable mirror reflectivity as function of wavelength, etc.) and to fully optimize the plasma-generation and optical systems with power recycling.

[1]V. Y. Banine, K. N. Koshelev, and G. H. P. M. Swinkels, J. Phys. D: Appl. Phys. **44**, 253001 (2011).
[2]A. Y. Vinokhodov, M. S. Krivokorytov, Y. V. Sidelnikov, V. M. Krivtsun, V. V. Medvedev, and K. N. Koshelev, Quantum Electron. **46**, 473 (2016).
[3]M. Richardson, C.-S. Koay, K. Takenoshita, C. Keyser, S. George, S. Teerawattansook, M. Al-Rabban, and H. Scott, Proc. SPIE **5374**, 447 (2004).
[4]J. van Schoot, K. van Ingen Schenau, C. Valentin, and S. Migura, Proc. SPIE **9422**, 94221F (2015).
[5]A. Pirati *et al*., Proc. SPIE **10143**, 101430G (2017).
[6]T. A. Brunner, X. Chen, A. Gabor, C. Higgins, L. Sun, and C. A. Mack, Proc. SPIE **10143**, 101430E (2017).
[7]S. Schreiber and B. Faatz, High Power Laser Sci. Eng. **3**, e20 (2015).
[8]S. Wieneke, S. Brückner, and W. Viöl, Phys. Plasmas **15**, 122508 (2008).
[9]E. Sterling and J. G. Lunney, AIP Conf. Proc. **1278**, 567 (2010).
[10]A. Yu. Vinokhodov, V. M. Krivtsun, A. A. Lash, V. M. Borisov, O. F. Yakushev, and K. N. Koshelev, Quantum Electron. **46**, 81 (2016).
[11]T. Krücken, K. Bergmann, L. Juschkin, and R. Lebert, J. Phys. D: Appl. Phys. **37**, 3213 (2004).
[12]M. Bayraktar, F. A. van Goor, K. J. Boller, and F. Bijkerk, Opt. Express **22**, 8633–8639 (2014).
[13]K. C. Johnson, J. Vac. Sci. Technol., B **34**, 041608 (2016).
[14]K. C. Johnson, U.S. patent 9,612,370 Bl (4 April 2017).
[15]V. Sizyuk and A. Hassanein, Laser Part. Beams **34**, 163 (2016).
[16]V. Sizyuk and A. Hassanein, Nucl. Fusion **53**, 073023 (2013).
[17]A. Hassanein, V. Sizyuk, T. Sizyuk, and S. Harilal, J. Micro/Nanolithogr., MEMS, MOEMS **8**, 041503 (2009).
[18]V. Sizyuk, A. Hassanein, and T. Sizyuk, J. Appl. Phys. **100**, 103106 (2006).
[19]S. I. Braginskii, in *Reviews of Plasma Physics*, edited by M. A. Leontovich (Consultants Bureau, New York, 1965), Vol. 1, p. 205.
[20]V. Sizyuk, A. Hassanein, V. Morozov, V. Tolkach, T. Sizyuk, and B. Rice, Numer. Heat Transfer, Part A **49**, 215 (2006).
[21]A. Hassanein, V. Sizyuk, V. Tolkach, V. Morozov, and B. J. Rice, J. Micro/Nanolithogr., MEMS, MOEMS **3**, 130 (2004).
[22]F. Wooten, *Optical Properties of Solids* (Academic Press, New York, 1972), p. 260.
[23]G. G. Grigoryan, A. G. Leonov, E. A. Manykin, A. A. Rudenko, M. G. Sitnikov, and A. N. Starostin, J. Exp. Theor. Phys. **97**, 678 (2003).
[24]A. Hassanein, V. Sizyuk, and T. Sizyuk, Proc. SPIE **6921**, 692113 (2008).
[25]V. Sizyuk and A. Hassanein, Phys. Plasmas **22**, 013301 (2015).
[26]G. V. Miloshevsky, V. A. Sizyuk, M. B. Partenskii, A. Hassanein, and P. C. Jordan, J. Comput. Phys. **212**, 25 (2006).
[27]A. Hassanein, V. Sizyuk, V. Tolkach, V. Morozov, and B. J. Rice, Proc. SPIE **5037**(2), 714 (2003).
[28]V. Sizyuk, A. Hassanein, and V. Bakshi, J. Micro/Nanolithogr., MEMS, MOEMS **6**, 043003 (2007).
[29]V. Sizyuk and A. Hassanein, Nucl. Fusion **49**, 095003 (2009).
[30]A. Hassanein, V. Sizyuk, V. Tolkach, V. Morozov, T. Sizyuk, B. J. Rice, and V. Bakshi, Proc. SPIE **5374**(1), 413 (2004).
[31]V. Morozov, V. Sizyuk, A. Hassanein, and V. Tolkach, Argonne National Laboratory Report ANL-ET-04/31, Argonne, IL, 2004.
[32]R. C. Spitzer, T. J. Orzechowski, D. W. Phillion, R. L. Kauffman, and C. J. Cerjan, J. Appl. Phys. **79**, 2251 (1996).
[33]V. Sizyuk, A. Hassanein, and T. Sizyuk, Laser Part. Beams **25**, 143 (2007).